Conf-820601--32

A MULTI-DIMENSIONAL ARBITRARY LAGRANGIAN-EULERIAN METHOD FOR DYNAMIC FLUID-STRUCTURE INTERACTION

CONF-820601--32

DE83 010577

C. Y. Wang* and W. R. Zeuch*

ABSTRACT

This paper describes an arbitrary Lagrangian-Eulerian method for analyzing fluid-structure interactions in fast-reactor containment with complex internal structures. The fluid transient can be calculated either implicitly or explicitly, using a finite-difference mesh with vertices that may be moved with the fluid (Lagrangian), held fixed (Eulerian), or moved in any other prescribed manner (hybrid Lagrangian Eulerian). The structural response is computed explicitly by two nonlinear, elastic-plastic finite-element modules formulated in corotational coordinates. Interaction between fluid and structure is accounted for by enforcing the interface boundary conditions. The method has convincing advantages in treating complicated phenomena such as flow through perforated structures, large material distortions, flow around corners and irregularities, and highly contorted fluid boundaries. Several sample problems are given to illustrate the effectiveness of this arbitrary Lagrangian-Eulerian method.

---

*Reactor Analysis and Safety Division
Argonne National Laboratory
9700 South Cass Avenue
Argonne, IL 60439

MASTER

DISTRIBUTION OF THIS DOCUMENT IS UNLIMITED

DISCLAIMER

This report was prepared as an account of work sponsored by an agency of the United States Government. Neither the United States Government nor any agency thereof, nor any of their employees, makes any warranty, express or implied, or assumes any legal liability or responsibility for the accuracy, completeness, or usefulness of any information, apparatus, product, or process disclosed, or represents that its use would not infringe privately owned rights. Reference herein to any specific commercial product, process, or service by trade name, trademark, manufacturer, or otherwise does not necessarily constitute or imply its endorsement, recommendation, or favoring by the United States Government or any agency thereof. The views and opinions of authors expressed herein do not necessarily state or reflect those of the United States Government or any agency thereof.

INTRODUCTION

Dynamic fluid-structure interaction analysis is very complex since it involves calculations of fluid transients and structural response. In the safety analysis of a typical Liquid Metal Fast Breeder Reactor (LMFBR), shown in Fig. 1, the problem of fluid-structure interaction is further complicated by the fact that (1) the structural components usually have both geometrical and material nonlinearities, (2) geometrical discontinuities like sharp corners and irregularities normally exist in the fluid region, (3) a wide spectrum of phenomena such as flow through perforated structures, large material distortions, multi-dimensional sliding interfaces, and flow around corners could occur during a Hypothetical Core Disruptive Accident (HCDA), and (4) the presence of the Upper Internal Structure (UIS), perforated dip plate, and other internals imposes difficulties on many numerical techniques.

In the past fifteen years substantial research effort has been devoted to the development of numerical methods and computer codes for performing the analysis of fluid-structure interaction. Most codes currently in use employ either a purely Lagrangian or a purely Eulerian approach for analyzing the fluid transient in conjunction with a Lagrangian method for calculating the structural response.

It is well known that, in the Lagrangian approach the mesh used for computing the coolant motion moves with the coolant. Difficulties arise when the physical situation involves large material distortions, flow around corners and irregularities, and outflow boundary conditions. In the Eulerian approach, on the other hand, the mesh used for the description of the coolant motion is fixed in space. Although such a mesh is ideal for treating excessive material distortions and outflow boundary conditions, difficulties also arise when the problem involves large structural displacement. Quite

often, considerable programming effort and cell-blending scheme are needed to deal with the irregular cells generated by the movement of the structures as they displace across the fixed Eulerian coordinates.

To eliminate the disadvantages and still maintain the advantages of both the Lagrangian and Eulerian methods, a two-dimensional arbitrary Lagrangian-Eulerian method [1] has been developed at Argonne National Laboratory (ANL). Based on this method, a computer code ALICE [2] has been written to analyze the fluid-structure transient in the LMFBR containment. The technique used for calculating the coolant motion is based on the ICED-ALE technique suggested by Hirt et al. [3]. In the ALICE analysis, the grid for computing fluid motions is a hybrid of Lagrangian and Eulerian discretizations. Thus, in the region where the coolant is expected to move extensively, the vertices of the fluid mesh can be made to move in an optimum manner. So that excessive mesh distortions can be completely eliminated by using a continuous rezoning process. Also, at the fluid-structure interface, the vertices of the fluid mesh can be made to move with the structure nodal points to simplify the computational procedure and to avoid irregular cell calculations.

Recently, the arbitrary Lagrangian-Eulerian method has been greatly extended. First, a three-dimensional pipe element [4,5] has been adopted [6] to simulate the motion of the support columns of the UIS. Secondly, capabilities have been developed to treat the internal thin shell, perforated dip plate, curved reactor bottom, and highly distorted core-gas bubble. Thus, the extended multi-dimensional arbitrary Lagrangian-Eulerian method has significant advantages in treating both complex excursion phenomena and complicated structural response. The resulting new version of the computer program, ALICE-II, is therefore, capable of performing an integrated, dynamic fluid-structure interaction analysis of LMFBR with complex internals.

Numerical calculations for the hydrodynamic solutions are separated into three phases. The first phase consists of an explicit Lagrangian calculation. The second phase, which is optional, contains an implicit iteration. The third phase, which is also optimal, rezones the mesh vertices to prescribed positions. The structural response is computed by two nonlinear, elastic-plastic, finite-element modules formulated in corotational coordinates. The first employs two-dimensional thin shell and quadrilateral continuum elements to model the reactor vessel and axisymmetric elastic-plastic solids. The second module utilizes a three-dimensional pipe element to calculate the buckling of the support columns that connect the upper internal structure to the reactor cover. All elements are capable of treating both material and geometric nonlinearities. Thus, the solution of a problem can be obtained in six different ways by the appropriate choice of the implicit or explicit time integration scheme, and the appropriate choice of the Lagrangian, Eulerian, or the arbitrary Lagrangian-Eulerian solution.

In this paper the equations used for the hydrodynamic and structural calculations are briefly described. Several problems dealing with dynamic fluid-structure interactions are given to illustrate the applications of this arbitrary Lagrangian-Eulerian method.

HYDRODYNAMICS

The basic differential equations used in the code are the conservation equations of continuum mechanics. Only nonturbulent flow is considered, and no external energy source is assumed to exist inside the flow region. Thus, the mass, momentum, and energy equations for the non-heat-conducting fluid are:

$$\frac{\partial \rho}{\partial t} + \frac{\partial}{\partial x_i} (\rho u_i) = 0 \ , \tag{1}$$

$$\frac{\partial}{\partial t} (\rho u_i) + \frac{\partial}{\partial x_j} (\rho u_i \ u_j) = \frac{\partial}{\partial x_i} \sigma_{ij} + \rho g_i \ , \tag{2}$$

$$\frac{\partial}{\partial t} (\rho E) + \frac{\partial}{\partial x_i} (\rho u_i \ E) = \frac{\partial}{\partial x_i} (\sigma_{ij} \ u_j) + \rho g_i \ u_i \ , \tag{3}$$

in which

$$E = I + \tfrac{1}{2} u_i \ u_i \ . \tag{4}$$

In Eqs. (1-4) ρ is the density; t the time; u_i the velocity component; g_i the component of gravitational accelerations; E the specific total energy; I is the specific internal energy; σ_{ij} is the stress tensor which is a function of the scalar pressure p and a deviatoric stress tensor $\bar{\sigma}_{ij}$, i.e.

$$\sigma_{ij} = - p\delta_{ij} + \bar{\sigma}_{ij} \ , \tag{5}$$

where δ_{ij} is Kronecker delta.

The deviatoric stress tensor can be written as

$$\bar{\sigma}_{ij} = \mu e_{ij} + \tfrac{1}{2} \lambda e_{\ell\ell} \ \delta_{ij} \ , \tag{6}$$

and

$$e_{ij} = \frac{\partial u_j}{\partial x_i} + \frac{\partial u_i}{\partial x_j} \ ,$$

in which μ and λ are the viscosity coefficients.

In the finite-difference technique, it is convenient to integrate Eqs. (1-3) over a control volume, V, and then convert the volume integrals to surface integrals over the control surfaces. Thus, in the integral form the mass, momentum, and the energy equations are:

$$\frac{d}{dt}\int_V \rho dV + \int_S \rho(u_i - U_i)\, n_i\, dS = 0 , \tag{7}$$

$$\frac{d}{dt}\int_{V'} \rho u_i\, dV' + \int_{S'} [\rho u_i\, (u_j - U_j) - \sigma_{ij}]\, n_j\, dS' - \int_{V'} \rho g_i\, dV' = 0 , \tag{8}$$

and

$$\frac{d}{dt}\int_V \rho E\, dV + \int_S \rho E(u_i - U_i)\, n_i\, dS - \int_S \sigma_{ij}\, u_j\, n_i\, dS - \int_V \rho g_i\, u_i\, dV = 0 . \tag{9}$$

In these equations u_i and U_i are the velocity components of the fluid and the bounding surface, respectively; n_i is the outward normal to the surface S; g_i is the gravitational acceleration. Note that when $u_i = U_i$, the convective terms in Eqs. (7-9) are vanished, and the equations are Lagrangian; when $U_i = 0$, the equations are Eulerian; and when $U_i \neq u_i$ and $U_i \neq 0$ the equations are hybrid Lagrangian-Eulerian.

At each time step, the fluid dynamic calculations are separated into three phases [3]. The first phase consists of an explicit Lagrangian calculation. Velocities are advanced by the pressure gradients, inertia, and viscous forces. The energy change due to inertia and viscous forces are also calculated in this phase. The energy change due to the pressure work will be performed after the second phase to permit the advanced-time pressure work to coincide with the advanced-time velocities.

The second phase performs an implicit calculation. The basic task of this calculation is to eliminate the Courant stability condition which limits the pressure waves to travel over one cell per time step. A Newton-Raphson iteration method is used to obtain advanced-time pressures which, in turn, are calculated by the discrepancies of the transport equations. Following the pressure changes at each iteration, densities, specific internal energies, and velocities are also adjusted. The converged pressures are used for the calculation of the pressure work to update the energy changes.

If, at this point of calculation, the mesh vertices are moved with the fluid, the result is Lagrangian. It is well known that the Lagrangian solutions are not accurate when the computing mesh is severely distorted. To avoid large mesh distortions and maintain an optimum mesh, the third phase performs a rezone calculation which allows the computing mesh to move in a prescribed manner. Convective fluxes due to the relative motions between the computing mesh and fluid are calculated to assure the conservations of mass, energy, and momentum.

TWO-DIMENSIONAL STRUCTURAL ANALYSIS

Most containment structures such as the radial shield, core barrel, core-support structure, and the primary vessel respond axisymmetrically. They are analyzed by a modified version of the finite-element program, WHAMS [7]. This program uses a corotational coordinate scheme in the numerical analysis and is best suited for large displacement, small strain, elastic-plastic dynamic problems.

In this scheme, Lagrangian coordinates of the element rotate but do not deform with the elements. The strain is linearly related to the displacement of the element relative to the Lagrangian coordinates. Similarly, the nodal

forces are linearly related to the element stresses. The original program, WHAMS, has the conical-shell element and axisymmetric triangle element which can be used to model complicated structural components.

The displacement field of the shell element consists of cubic transverse displacements and linear axial displacements. Resultant forces are computed by five-point numerical integrations across the depth of the element. The triangle continuum element uses linear displacement fields. It can be used to simulate fluid or elastic-plastic solids. Recently, a quadrilateral fluid element and a quadrilateral elastic-plastic element have been added to the program [2].

THREE-DIMENSIONAL STRUCTURAL ANALYSIS

A three-dimensional general purpose pipe element, which is developed using a corotational coordinate formulation [5], was used to model the buckling of the UIS support columns subjected to the upward force transmitted from the assembly portion of the UIS. Each element has eight degrees of freedom per node. Six degrees of freedom, three displacements, and three rotations, describe the flexural motion in three-dimensional space. The remaining two degrees of freedom describe the axisymmetric breathing mode in terms of hoop displacement and wall bending rotation generated by the pressure wave transmitted from the fluid inside the pipe. In the calculation of the UIS column motion, these two degrees of freedom can be ignored, reducing the problem to the case where no fluid is inside the pipe.

Three types of coordinate systems are used to describe the pipe system: a fixed global system of coordinates (X, Y, and Z); a nodal body coordinate system ($\bar{x}$, $\bar{y}$, and $\bar{z}$) associated with each node, their initial orientation coinciding with the principal directions of the nodal mass moment of inertia

tensor and rotating with the nodes; and an element (corotational) coordinate system (x, y, and z) associated with each element. The unit vectors $\hat{b}_1$, $\hat{b}_2$, and $\hat{b}_3$ are associated with the nodal body coordinates $\bar{x}$, $\bar{y}$, and $\bar{z}$, respectively. Similarly, the unit vectors $\hat{e}_1$, $\hat{e}_2$, and $\hat{e}_3$ are associated with the element coordinates x, y, and z, respectively.

A generic pipe element with nodes I and J at its ends is shown in Fig. 2a. The x-axis always joins the two nodes I and J, so that it rotates with the element but does not deform with the element. The y and z axes are in the plane of cross-section of the pipe and are considered to rotate with the element such that their rotation is the average of the rotation of the two nodes, I and J, about the x-axis.

Equations of Motion

The translational equation of motion in global coordinates for each node is

$$\rho_i \ddot{u}_i = F_i^{ext} - F_i^{int} , \tag{10}$$

where i = 1, 2, and 3 for the global X, Y, and Z direction; ρ_i is the translational mass of the node in the i-direction; $\ddot{u}_i$ is the translational acceleration of the node in the i-direction; F_i^{ext} is the sum of all external forces applied to the node in the i-direction; and F^{int} is the sum of internal nodal forces due to deformation of all elements connected to the node.

The rotational equations of motion are expressed in the nodal (body) coordinate system of each node and are given by

$$I_{\bar{x}\bar{x}}\,\dot{\omega}_{\bar{x}} + (I_{\bar{z}\bar{z}} - I_{\bar{y}\bar{y}})\,\omega_{\bar{y}}\,\omega_{\bar{z}} = M_{\bar{x}}^{ext} - M_{\bar{x}}^{int}$$

$$I_{\bar{y}\bar{y}}\,\dot{\omega}_{\bar{y}} + (I_{\bar{x}\bar{x}} - I_{\bar{z}\bar{z}})\,\omega_{\bar{x}}\,\omega_{\bar{z}} = M_{\bar{y}}^{ext} - M_{\bar{y}}^{int} \qquad (11)$$

$$I_{\bar{z}\bar{z}}\,\dot{\omega}_{\bar{z}} + (I_{\bar{y}\bar{y}} - I_{\bar{x}\bar{x}})\,\omega_{\bar{x}}\,\omega_{\bar{z}} = M_{\bar{z}}^{ext} - M_{\bar{z}}^{int} ,$$

where $I_{\bar{x}\bar{x}}$, $I_{\bar{y}\bar{y}}$, and $I_{\bar{z}\bar{z}}$ are the principal mass moments of inertia of the node; $\dot{\omega}_{\bar{x}}$, $\dot{\omega}_{\bar{y}}$, and $\dot{\omega}_{\bar{z}}$ are the angular accelerations of the node about the $\bar{x}$-, $\bar{y}$-, and $\bar{z}$-axes; $\omega_{\bar{x}}$, $\omega_{\bar{y}}$, and $\omega_{\bar{z}}$ are the angular velocities of the node about the $\bar{x}$-, $\bar{y}$-, and $\bar{z}$-axes; $M_{\bar{x}}^{ext}$, $M_{\bar{y}}^{ext}$, and $M_{\bar{z}}^{ext}$ are the sum of all external moments applied to the node about the $\bar{x}$-, $\bar{y}$-, and $\bar{z}$-axes; $M_{\bar{x}}^{int}$, $M_{\bar{y}}^{int}$, and $M_{\bar{z}}^{int}$ are the sum of internal moments about the $\bar{x}$-, $\bar{y}$-, and $\bar{z}$-axes due to deformation of all elements connected to the node.

Deformation Displacements

Because the deformation displacements are computed in the corotational coordinate system, the deformations become independent of the rigid body rotation of the element. This element, therefore, is suitable for problems involving large rotations of the centerline. Within the corotational coordinate system, the deformation displacements are defined as

$$\{d\}^T = \{\delta_{IJ},\ \gamma_{xIJ},\ \gamma_{yI},\ \gamma_{zI},\ \gamma_{yJ},\ \gamma_{zJ}\} , \qquad (12)$$

where δ_{IJ} is the elongation in the pipe axis; γ_{xIJ} is the torsional rotation of the pipe midline; and γ_{yI}, γ_{zI}, γ_{yJ}, and γ_{zJ} are the bending rotations of the pipe midline.

Strain-Displacement Relations

The axial strain at a layer in the pipe shell is given by

$$\varepsilon_x = \varepsilon_m - y \frac{\partial^2 v_y}{\partial x^2} - z \frac{\partial^2 v_z}{\partial x^2} , \tag{13}$$

where ε_m is the strain of the pipe centerline; and v_y and v_z are the corotational components of the displacements of the pipe midline, as shown in Fig. 2 (b-c).

The shear strain is given by

$$\varepsilon_{x\theta} = r \frac{\partial \gamma_x}{\partial x} , \tag{14}$$

where γ_x is the rotation about the x-axis.

Since the x-axis connects nodes I and J at all times, the transverse displacement of the pipe midline can be expressed completely in terms of the nodal bending rotations. Thus

$$v_y = \phi_I \gamma_{zI} + \phi_J \gamma_{zJ} , \tag{15}$$

$$v_z = -\phi_I \gamma_{yI} - \phi_J \gamma_{yJ} , \tag{16}$$

$$\gamma_x = \beta_I \gamma_{xI} + \beta_J \gamma_{xJ} , \tag{17}$$

where

$$\phi_I = \ell(\xi - 2\xi^2 + \xi^3) \quad , \quad \phi_j = \ell(\xi^3 - \xi^2) ,$$

$$\beta_I = 1 - \xi \quad , \quad \beta_J = \xi \quad , \text{ and } \quad \xi = x/\ell . \tag{18}$$

The negative sign in Eq. (16) results from the fact that, for a right handed system of coordinates, a positive rotation about the y-axis causes a negative displacement in the z-direction.

Force-Stress Relations

The nodal internal force vector conjugate to the nodal displacement vector of Eq. (12) is

$$\{F^{int}\}^T = \{F_{xI},\ M_{xI},\ M_{yI},\ M_{zI},\ M_{yJ},\ M_{zJ}\} \ . \tag{19}$$

Using the principle of virtual work, we obtain

$$\{d\}^T\ \{F^{int}\} = \int_V (\varepsilon_x\ \sigma_x + \varepsilon_\theta\ \sigma_\theta + \varepsilon_{x\theta}\ \sigma_{x\theta})\ dV \ . \tag{20}$$

Substituting Eqs. (12) and (19) in the left hand side of Eq. (20), and Eqs. (13-18) in the right hand side of Eq. (20), then equating the coefficients of ε_m, γ_{xIJ}, γ_{yI}, γ_{zI}, . . ., γ_{yJ}, γ_{zI}, . . . etc. yields the nodal internal forces in terms of the stresses as

$$\begin{aligned}
F_{xK} &= \frac{1}{\ell}\int_V \sigma_x\ dV \\
M_{yK} &= -\int_V r\sin\theta\ \phi_{K,xx}\ \sigma_x\ dV \\
M_{zK} &= \int_V r\cos\theta\ \phi_{K,xx}\ \sigma_x\ dV \\
M_{xK} &= \int_V r\ \beta_{K,x}\ \sigma_{x\theta}\ dV \ ,
\end{aligned} \tag{21}$$

where K = I, J.

Equilibrium of the element gives the remaining nodal internal forces

$$M_{xI} = -M_{xJ} \quad , \quad F_{xI} = -F_{xJ} \quad ,$$

$$F_{yJ} = -\frac{M_{yI} + M_{yJ}}{\ell} \quad , \quad F_{yI} = -F_{yJ} \quad , \tag{22}$$

$$F_{zJ} = \frac{M_{zI} + M_{zJ}}{\ell} \quad , \quad \text{and} \quad F_{zI} = -F_{zJ} \quad .$$

The integrals for the nodal force, Eq. (21), are evaluated numerically using Gaussian quadrature. The pipe forces are then transformed to the global coordinate system, while the pipe moments are transformed to the body coordinate system before their assembly into the internal force matrix to be used in the equations of motion.

Application of the equations of motions as described above results in the new acceleration. These equations of motion are integrated in time by the Newmark β-method, with $\beta = 0$. This method is almost identical to the central difference method.

FLUID STRUCTURE INTERACTION

As mentioned earlier, the hydrodynamic equations are integrated with either an implicit or explicit scheme, whereas the governing equations for the structural analysis are integrated with only an explicit scheme. Thus, both implicit-explicit or explicit-explicit coupling calculations can be performed by the arbitrary Lagrangian-Eulerian method. The coupling calculations are implemented in two separate steps. The fluid supplies the structure with a pressure loading, which causes the structure to move. In return, the

structure gives the fluid a moving boundary condition at the fluid-structure interface. The optimum choice of the mesh movement for fluid-structure interaction problems is to move the vertices of the fluid cells adjacent to a structure along with those of the structure. Thus, the movement of the structure nodes relative to fixed vertices will not create any irregular cells for the fluid calculation.

The boundary conditions at the fluid-structure interface require that the fluid can slide freely along the structure surface, but must move together with the structure in the normal direction. Figure 3 shows the structural segments with nodal points 1, 2, and 3 located on the side of the fluid cells A and B with corresponding fluid nodes 1', 2', and 3'. We assume that the normal direction at point 2 is determined by the line connecting points 1 and 3. Thus, the boundary conditions, requiring that the fluid velocities to be changed from $u_{2'}$ and $v_{2'}$ to $u'_{2'}$ and $v'_{2'}$, are

$$u'_{2'} = u_2 \sin^2\theta - v_2 \sin\theta \cos\theta + u_{2'} \cos^2\theta + v_{2'} \sin\theta \cos\theta , \tag{23}$$

and

$$v'_{2'} = - u_2 \sin\theta \cos\theta + v_2 \cos^2\theta + u_{2'} \sin\theta \cos\theta + v_{2'} \sin^2\theta , \tag{24}$$

where

$$\theta = \cos^{-1}\left[\frac{x_3 - x_1}{\sqrt{(x_3 - x_1)^2 + (y_3 - y_1)^2}}\right] ,$$

and u_2 and v_2 are the radial and axial velocity components at structural nodal point 2.

Since the vertices of the fluid cell adjacent to the structure have been moved with different velocities from the structural nodal points, a rezone calculation is required in the third phase to compute the convective flux due to the relative motion between the fluid and the computing mesh as the fluid vertices move back to coincide with the structural nodal points.

NUMERICAL STABILITY AND SUB-CYCLING

In order to ensure numerical stability, limitation of time steps for both hydrodynamic and structural calculations must be given. The time step δt_h, chosen for the hydrodynamic analysis, must satisfy the modified "Courant Condition". The restriction is that fluid must not be permitted to flow across more than one computational cell in one time step; that is

$$\delta t_h < \left| \frac{V}{u^R \, dS} \right|_{min} , \tag{25}$$

where V is the control volume for either the mass or the momentum calculation, and u^R is the relative velocity between the computing mesh and the fluid in the normal direction of the surface dS.

In the axisymmetric structural-dynamics analysis the time step δt_s, employed for the explicit numerical integration must satisfy the following requirement

$$\delta t_s \leq \text{Min} \left(\frac{B\ell}{\sqrt{E/\rho}} \, , \, \frac{\beta \ell^2}{6\sqrt{Eh^2/12\rho}} \right), \tag{26}$$

where β is a reduction factor usually between 0.5 and 0.8; ℓ is the element length; E is Young's modulus of elasticity; h is the element thickness; and ρ is the density of the solid material.

For the problem involving calculation of the UIS movement, the classical Fourier theories of numerical stability are not applicable in the three-dimensional analysis of the UIS support columns, because of the quadratic combination of velocities in Eq. (11). Therefore, stability limits corresponding to the linearized analysis can only be served as a guideline for the stable time step. The destabilizing effects of nonlinearities can usually be overcome by further reducing the time step obtained from the linearized analysis.

When the element has both axial and flexural stiffness such as the pipe element used for simulating the UIS support columns the time step $\delta t_s'$ can be estimated from

$$\delta t_s' \leq \text{Min}\left(\frac{\beta \ell}{\sqrt{E/\rho}} \ , \ \frac{\beta \ell^2}{6 r_g \sqrt{E/\rho}}\right), \tag{27}$$

where r_g is the radius of gyration of the pipe cross section.

Because the hydrodynamic program usually uses an implicit integration scheme while the structural-dynamics program utilizes an explicit integration procedure, δt_h is usually larger than δt_s (or $\delta t_s'$). Thus, within each time step, several structural dynamics calculations must be performed in order to match one hydrodynamic calculation. For instance, the number of structural steps N (known as sub-cycles) used in the axisymmetric structural analysis can be determined by

$$N = I(\delta t_h / \delta t_s) + 1 \ , \tag{29}$$

where I denotes the integer part of the ratio.

If the analysis involves calculations of motions of the UIS support columns, the number of sub-cycles N′ used in the three-dimensional structural analysis can be estimated from Eq. (29) by simply replacing δt_s by $\delta t_s'$.

EXAMPLES

Three problems are presented to illustrate this arbitrary Lagrangian-Eulerian method. The first one deals with a transient fluid-structure interaction problem selected by the APRICOT (Analysis of PRImary COntainment Transient) project. This project, initiated by the U.S. Department of Energy, involves several reactor safety analysis groups around the world. Each is invited to perform independent calculations of identical problems in order to verify capabilities of large computer codes used for the LMFBR safety analysis. Presently, the APRICOT project is at the Phase 3 stage, aiming at validation of structural and fluid-structural-coupling capabilities, using some simple and well defined problems. Here, we select problem 2B to demonstrate the flexibility of the arbitrary Lagrangian-Eulerian method.

Figure 4 shows the configuration of this problem in which an annulus of fluid is subjected to a prescribed pressure history of the inner surface, while the outer surface is restrained by a thin cylindrical shell. The applied pressure was constant at 8 MPa. The fluid properties were described by a simple equation of state with a pressure cut-off at 0, i.e., $P_{min} = 0.0$. The thickness of the thin shell is 0.01693 cm.

As we mention in the introductory section that the solution of the fluid transient can be obtained in six different ways, by the appropriate choice of the implicit or explicit scheme, and the appropriate choice of the Lagrangian, Eulerian, or hybrid Lagrangian-Eulerian solution. Because of the space limitation, we will present results obtained from two representative

calculations, using the explicit hybrid Lagrangian-Eulerian and implicit Eulerian schemes, respectively. In the hybrid analysis the prescribed radial velocity of each interior node is proportional to the shell velocity, depending on the ratio of its radial coordinate to the shell radial coordinate. However, in the Eulerian calculation only nodes adjacent to the thin shell are assumed to move with the structure, while other nodes are kept stationary. Since no experimental data is available for this problem, solutions obtained from the ICECO-CEL code [7] are given for the purpose of comparison.

Figure 5 presents a comparison of predicted fluid pressures on the shell as a function of time. Each pressure profile is comprised of four major peaks. The first one is generated by the incident wave, whereas the other three are caused by successive reflections between the shell and the source. It can be seen that the agreement among these three pressure curves is quite good - not only the peak values but also the wave arrival times. Also, as we expected, the explicit hybrid Eulerian-Lagrangian calculation exhibits more wave phenomena in its pressure profile, and appears to be more oscillatory. On the other hand, the implicit Eulerian calculation of the arbitrary Lagrangian-Eulerian technique provides a relatively smooth solution and almost duplicates the result of the ICECO-CEL code. Figure 6 shows the shell velocity as a function of time. Again, except for the detailed wave phenomena, the agreement among these three solutions is very good.

The second problem deals with a study of the effects of a perforated plate on the slug impact load and containment response. The mathematical model used in the ALICE analysis is shown in Fig. 7. The reactor configuration consists of a primary vessel, a core barrel, a perforated dip plate, and a movable reactor cover with holddown bolts. Marker particles are

used to represent coolant. Two calculations have been performed with the ALICE code: one with and the other without the perforated dip plate.

Figure 8 presents reactor configurations at three different times for the case with the perforated plate. These configurations show how the core-gas bubble expands and how the core barrel and primary vessel deform during the excursion. In addition, Fig. 8 indicates significant flow blockage near the bottom of the perforated plate.

Reactor configurations for the case without the perforated plate are shown in Fig. 9. By comparing the configurations for the two cases given in Figs. 8 and 9, it is evident that the perforated plate has the effect of (1) confining the HCDA bubble expansion, (2) slowing down the upward movement of the coolant slug, (3) changing the smooth coolant free surface to a relatively turbulent one, and (4) reducing the slug-impact loads and the upper vessel wall deformation. However, the increase in core barrel deformation owing to the slower core-gas-bubble expansion, which results from the suppression effect of the perforated plate, is quite small.

From this second study, it can be concluded that the perforated plate does play an important role in the overall containment response; in particular, it has a mitigating effect on the slug impact and upper vessel deformation.

The third problem investigates the response of a typical LMFBR during an HCDA. Figure 10 shows the mathematical model used in the analysis. It consists of a primary vessel with a curved bottom, a movable Upper Internal Structure (UIS), a segmented steel radial shield, a core barrel, and a core-support structure (CSS). Marker particles are used to represent the coolant.

Note that the support columns that connect the UIS with the reactor cover are not shown in the mathematical model. However, the deformations of the

support columns can be perceived from the movement of the UIS. These deformations, generated by the buckling of the support columns, are calculated by the three-dimensional pipe element. The source pressure in the core-gas bubble is computed from the pressure-volume relationships rather than the pressure-time histories, since the latter are not known a priori during an HCDA. The initial core pressure was taken to be about 26.3 MPa.

Figure 11 shows reactor configurations at three different times. These configurations illustrate: (1) how the coolant disturbance occurs in the bottom portion of the reactor from pressure waves propagating downward through the opening of the CSS, (2) how the core-gas bubble expands and is distorted as it encounters the sharp corners of various internal structures, (3) how the UIS is displaced upward and how it interacts with the core-gas bubble, as well as with the surrounding fluid, (4) how the fluid moves and how the free surface impinges on the reactor cover, and (5) how the radial shield, core barrel and the primary vessel are deformed during the course of the excursion. These deformations can be seen from the movements of cell vertices adjacent to these structures.

Figure 12 gives the time history of the upward force acting on the UIS. Figure 13 presents the displacement of the UIS as a function of time. Such displacement is caused by the buckling of the support columns.

SUMMARY AND CONCLUSION

It has been demonstrated that the arbitrary Lagrangian-Eulerian method described above is very effective for analyzing dynamic fluid-structure interactions in fast reactor containment. The method is extremely versatile and includes options of Lagrangian, Eulerian, or hybrid Lagrangian-Eulerian computational schemes, with time integration performed either implicitly or

explicitly. Using the arbitrary Lagrangian-Eulerian hydrodynamic technique not only eliminates the mesh distortion problem associated with a purely Lagrangian technique, but also alleviates the difficulty of treating the fluid-structure interface encountered by the purely Eulerian method. Furthermore, utilization of the co-rotational finite-element formulation in the structural analysis enables the modeling of complex structures subject to large displacements in two- and three-space dimensions.

The arbitrary Lagrangian-Eulerian method has other important features: (1) it employs the complete hydrodynamic equations in the formulation, including both the nonlinear convective and viscous-dissipation terms. (2) It is highly user-oriented, and can provide a stable solution throughout the entire excursion without using only complementary mechanism such as artificial viscosities, damping coefficients, rezonings, and mesh stabilizations. This is a decided advantage for applying the method to both parametric studies and production runs. (3) It has the capability of treating flow through coolant passageways of the UIS and perforated structures, which is of significance in the safety analysis of LMFBRs.

In the first sample problem, the analytical predictions have been compared with ICECO-CEL results. More importantly, the arbitrary Lagrangian-Eulerian method and the ALICE code system have also been validated against many experimental data [see Refs. 1, 2]. Good agreement with experiments and established analytical methods demonstrates that the ALICE code system can predict accurately the response of primary containment systems generated by dynamic fluid-structure interactions.

ACKNOWLEDGEMENTS

This work was performed in the Engineering Mechanics Program of the Reactor Analysis and Safety Division at Argonne National Laboratory under the auspices of the U.S. Department of Energy.

REFERENCES

1. Chu, H. Y., "Arbitrary Lagrangian-Eulerian Method for Transient Fluid-Structure Interactions," Nuclear Technology, Vol. 51, No. 3, pp. 363-377, December, 1980.

2. Chu, H. Y., "ALICE: A Hybrid Lagrangian Eulerian Code for Calculating Fluid-Structural Interaction Transients in Fast Reactor Containment," ANL-79-72, Argonne National Laboratory, August, 1979.

3. Hirt, C. W., Amsden, A. A., and Cook, J. L., "An Arbitrary Lagrangian-Eulerian Computing Method for All Fluid Speed," J. Comp. Phys., Vol. 14, pp. 227, 1974.

4. Belytschko, T. B., et al., "Large Displacement, Transient Analysis of Space Frames," Int. J. Num. Meth. Eng., Vol. 11, pp. 65, 1977.

5. A-Moneim, M. T., "Three-Dimensional Finite Element Formulation for Elastic-Plastic Nonlinear Analysis of Piping Systems," Nuclear Technology, Vol. 51, No. 3, pp. 464-475, December, 1980.

6. Chu, H. Y. and Chang, Y. W., "Incorporation of Structural Part of SHAPS Code into the ALICE Code," ANL-RDP-82, p. 1.20, February, 1980.

7. Belytschko, T. B. and Mullen, R., "WHAMS - Program for Transient Nonlinear Analysis of Structures and Continua," Department of Civil Engineering Report, Northwestern University, 1978.

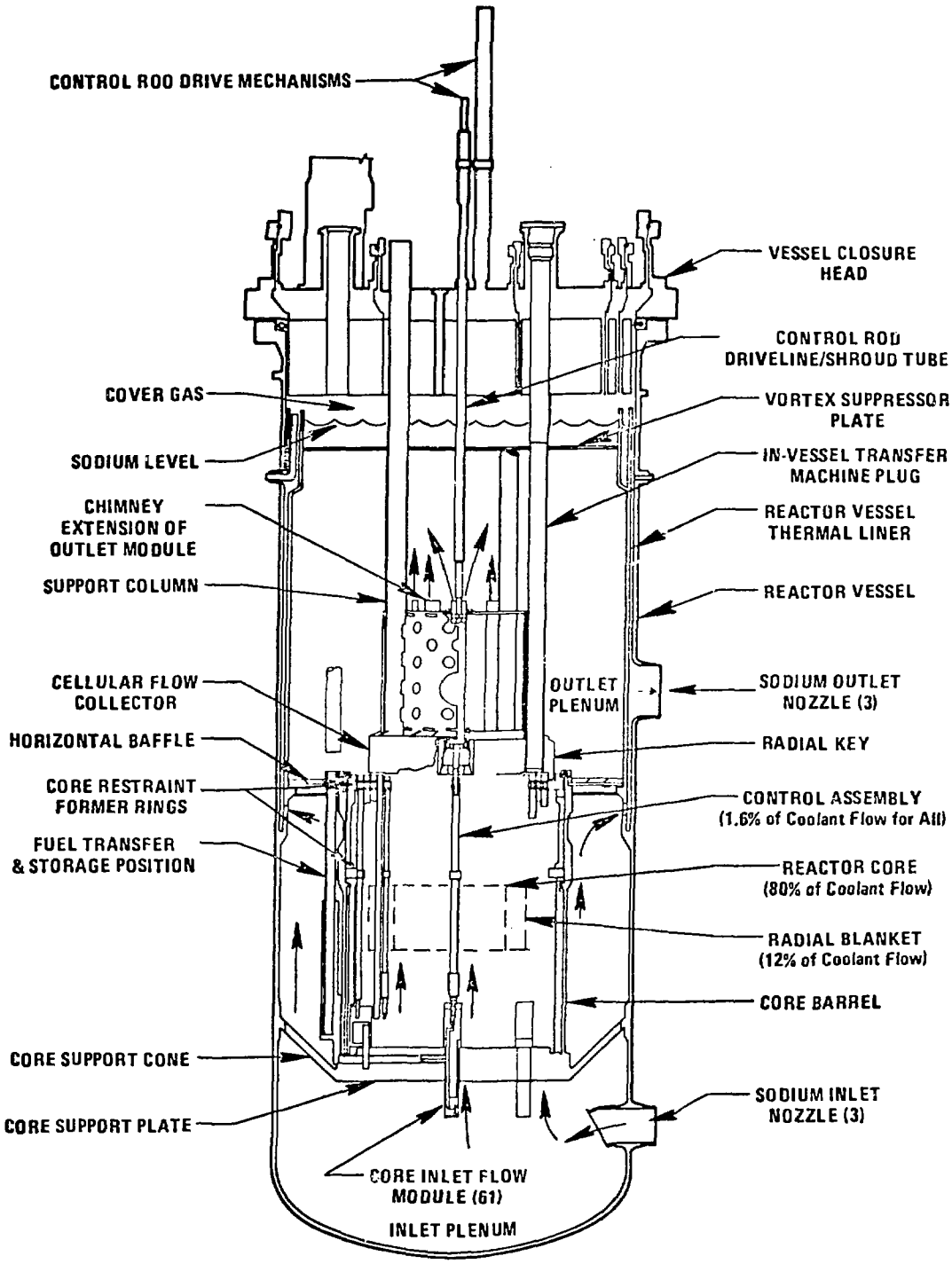

Fig. 1. Typical Configuration of an LMFBR.

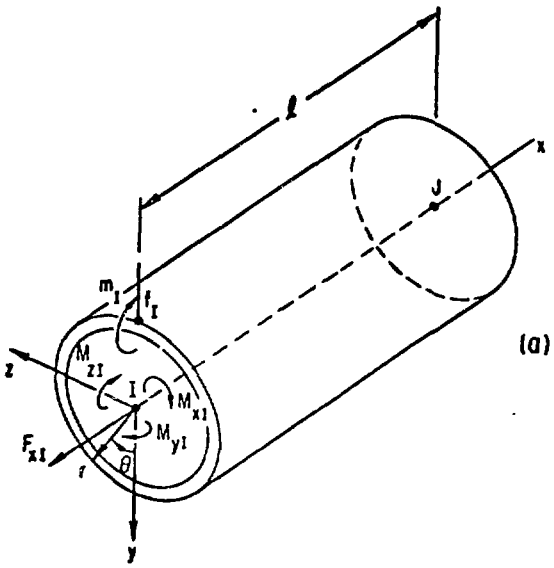

(a) Node and Element Coordinate Nomenclature and Nodal Forces

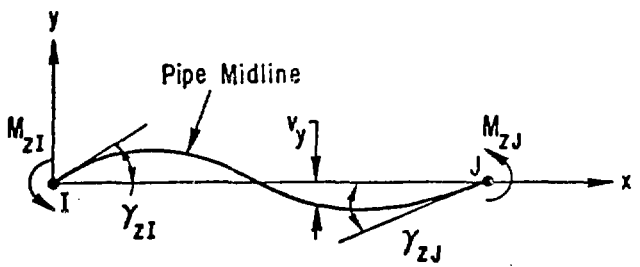

(b) Deformed Pipe Midline in the x-y Plane

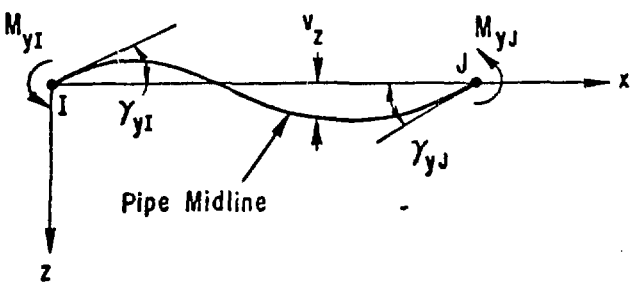

(c) Deformed Pipe Midline in the x-z Plane

Fig. 2. Generic Pipe Element and its Deformed Configurations.

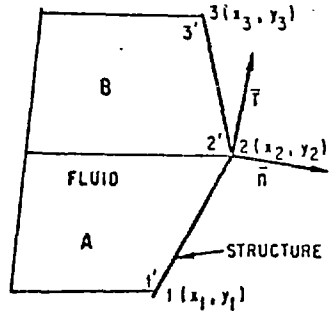

Fig. 3. Fluid-structure Coupling Calculation.

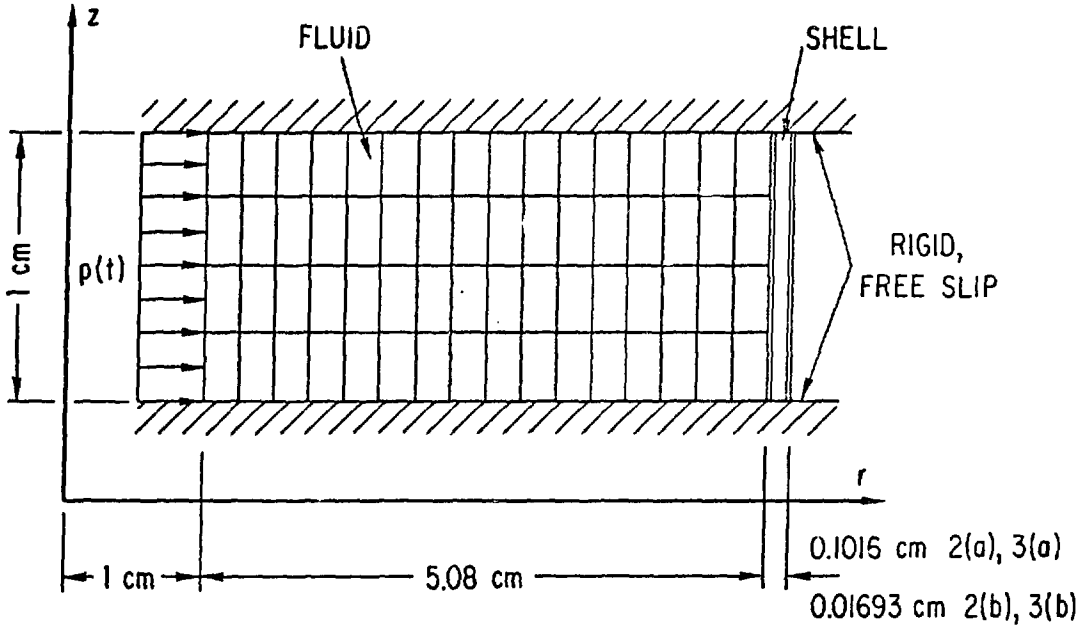

Fig. 4. Configuration of the APRICOT Problem 2B.

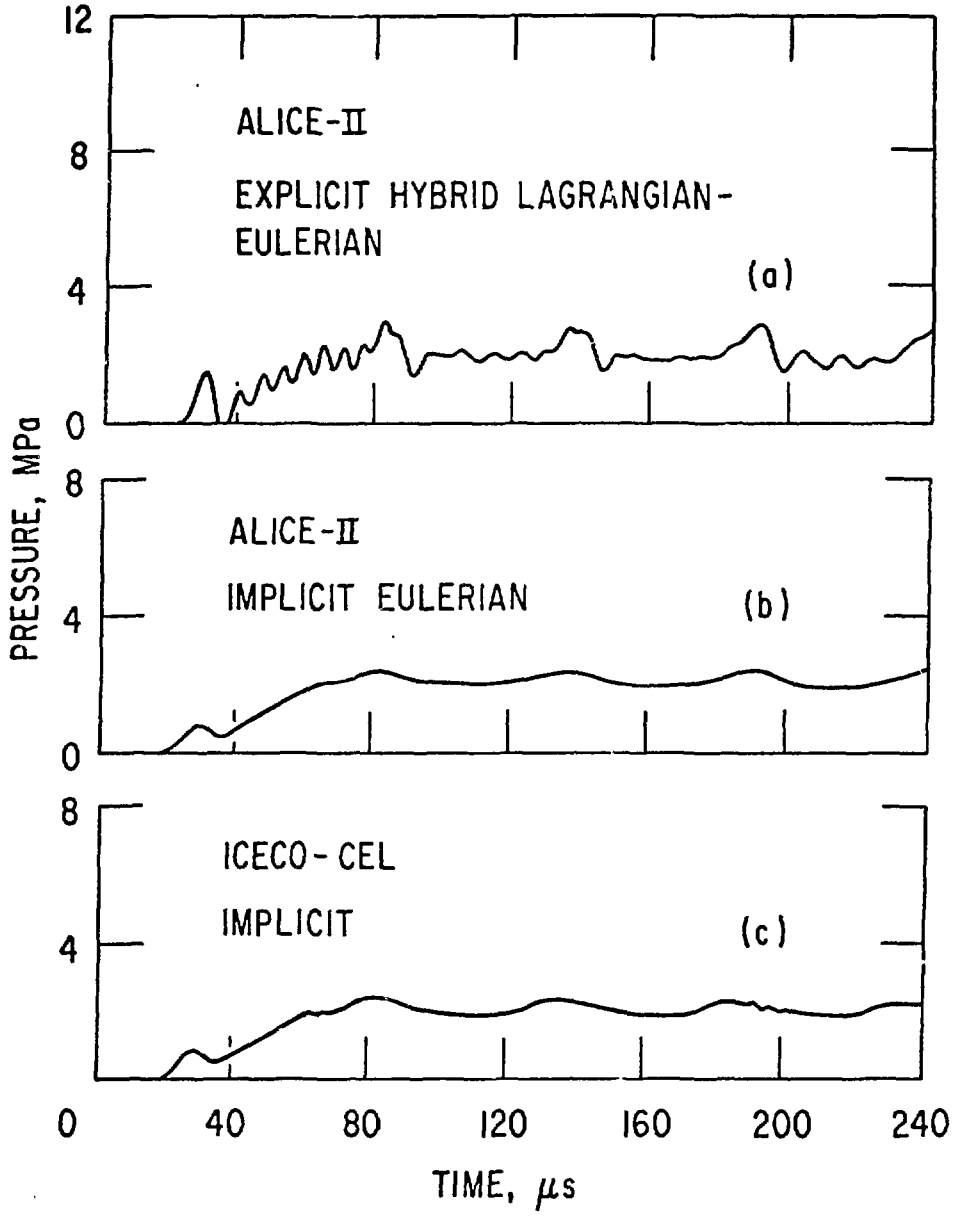

Fig. 5. Comparison of Fluid Pressures on the Shell as a Function of Time.

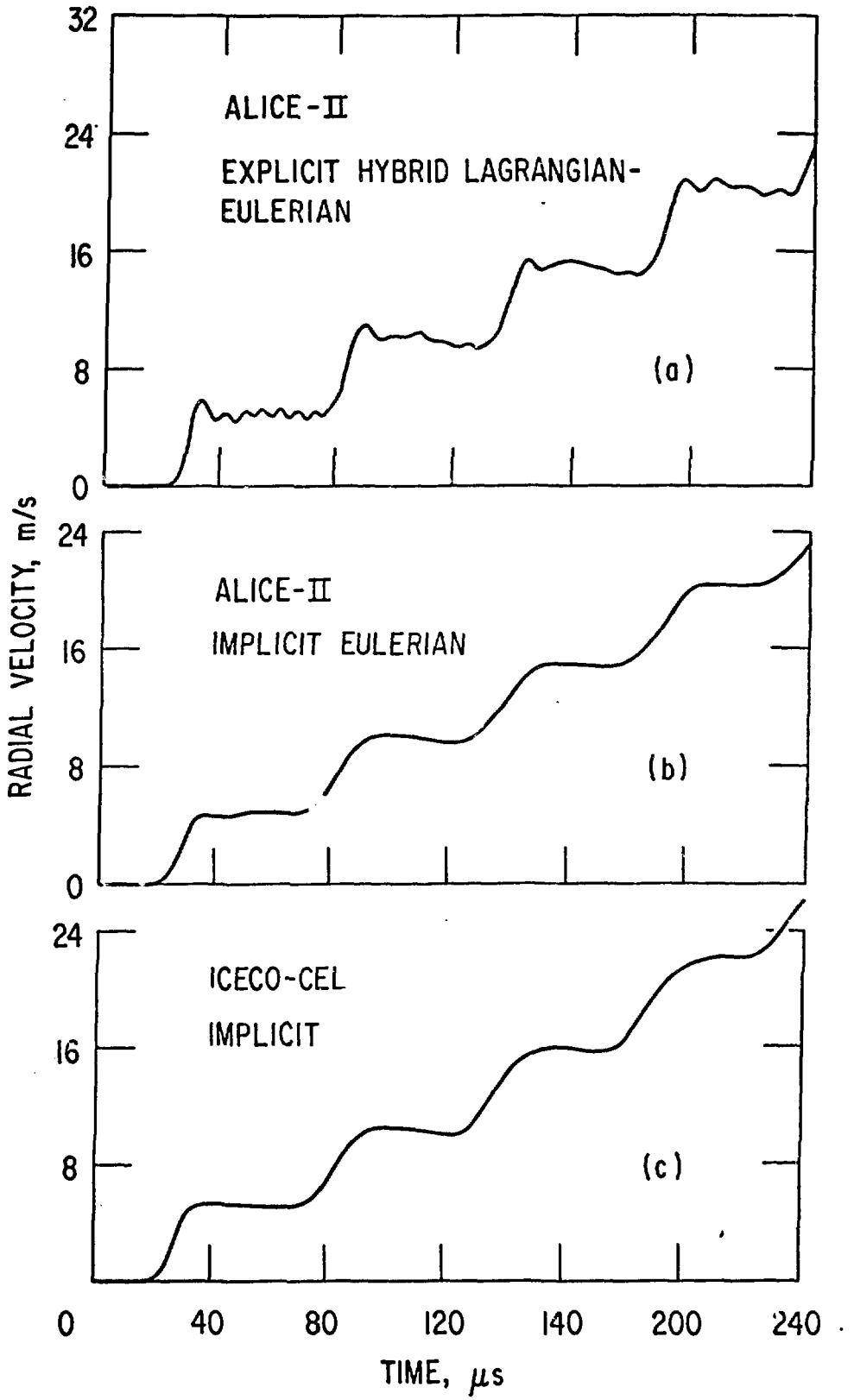

Fig. 6. Comparison of Shell Velocities as a Function of Time.

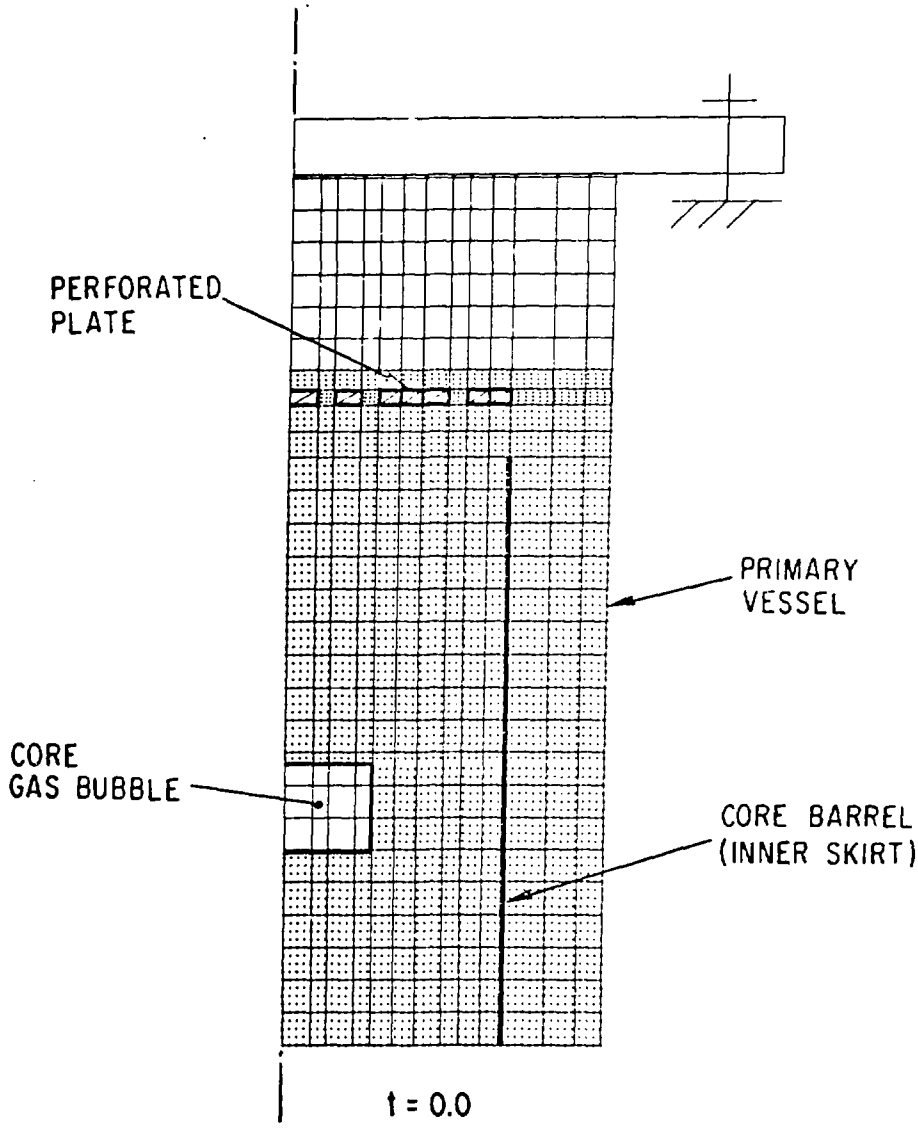

Fig. 7. Initial Configuration Used in the ALICE-II Analysis.

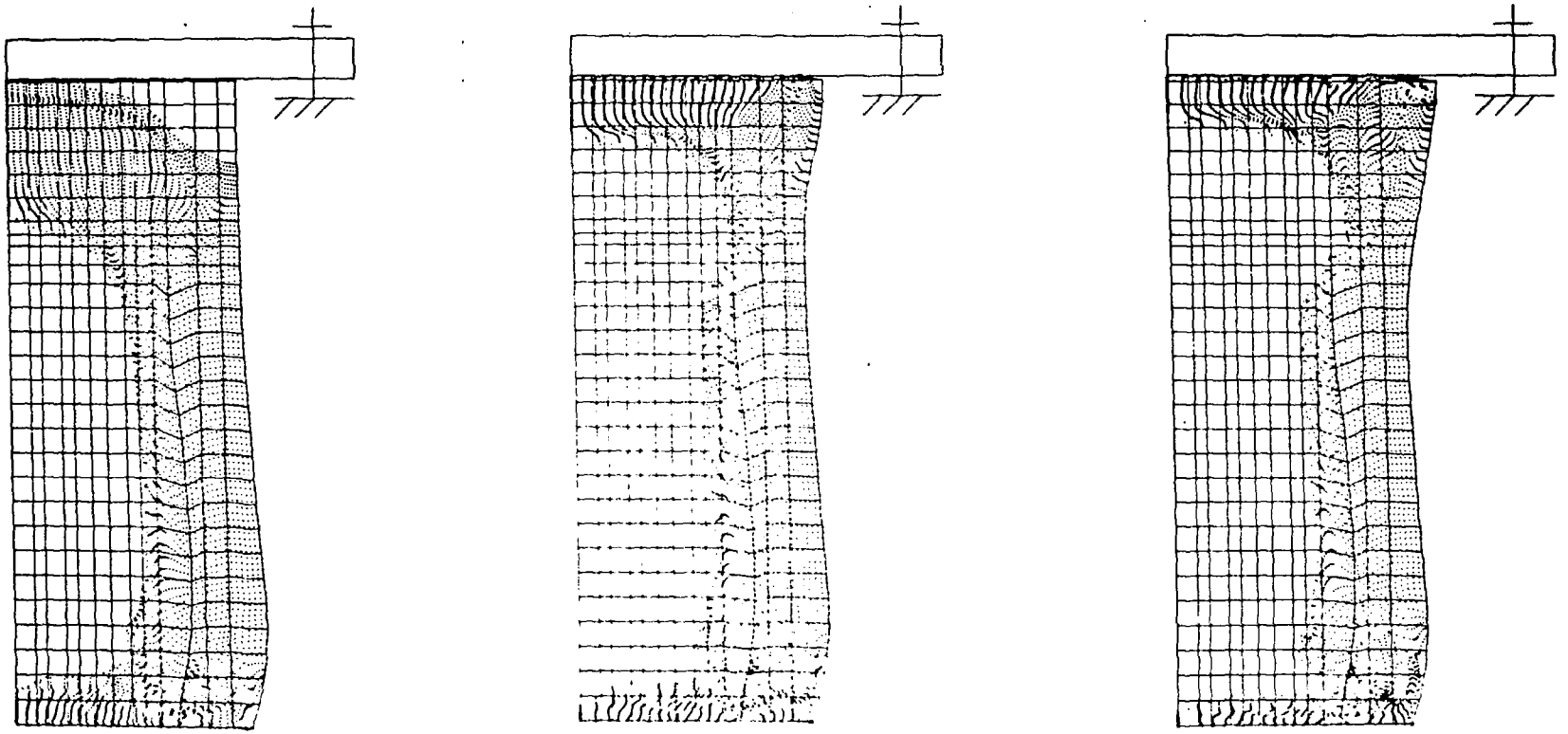

Fig. 8. Reactor Configurations at Three Different Times: With the Perforated Plate.

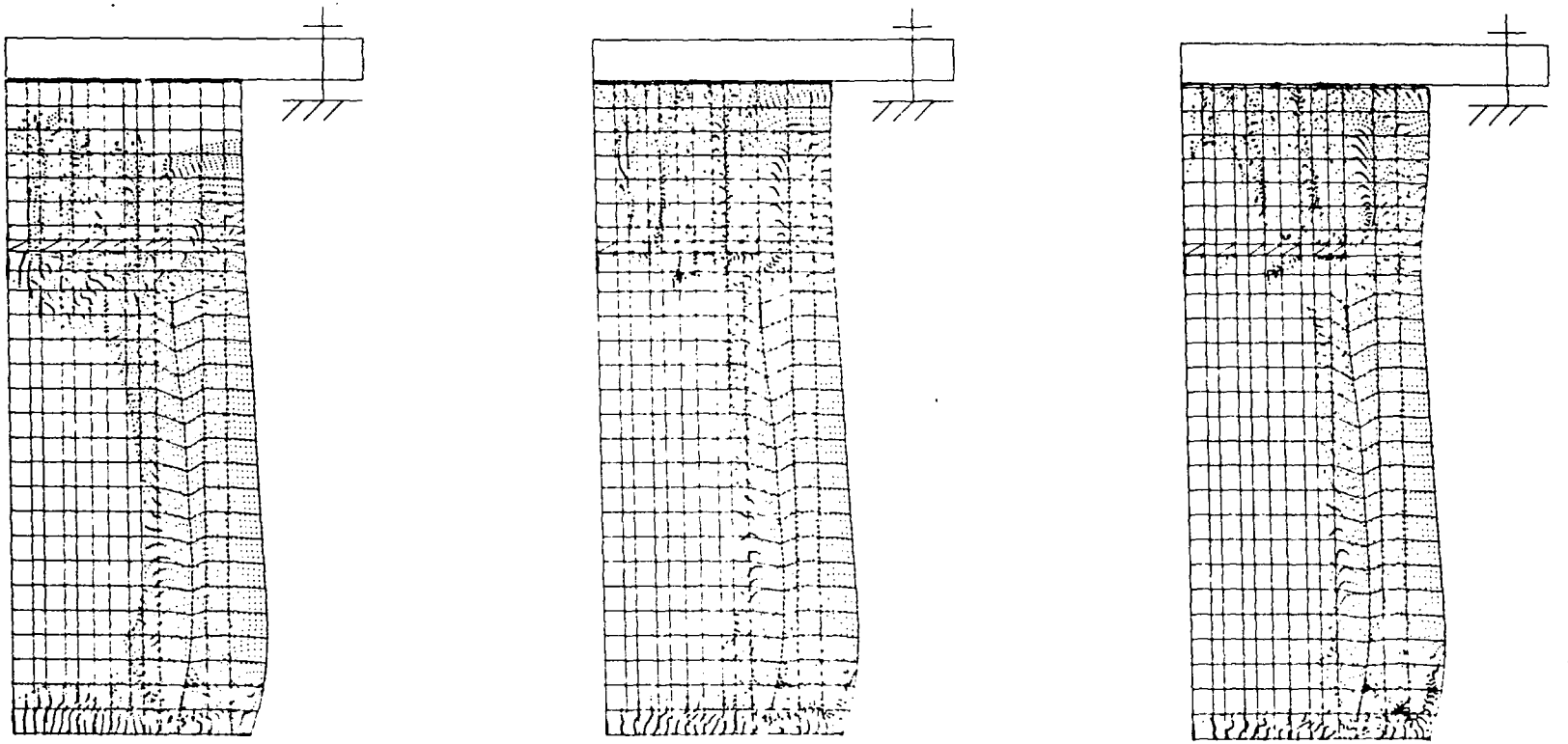

Fig. 9. Reactor Configurations at Three Different Times: Without the Perforated Plate.

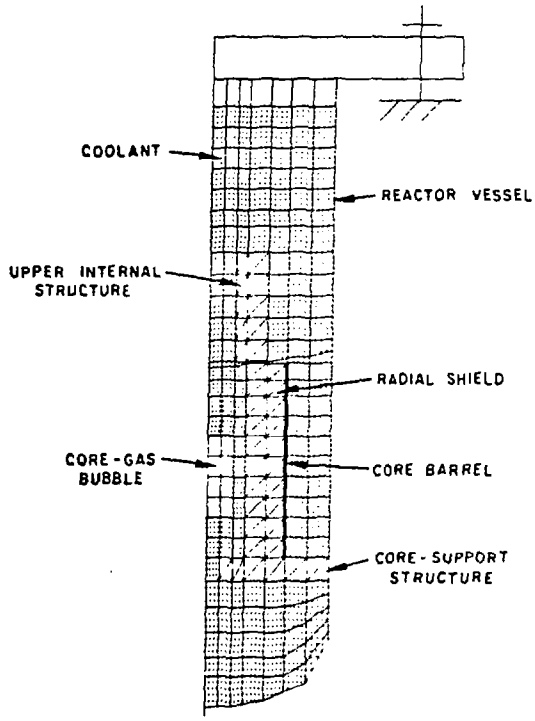

Fig. 10. Initial Configuration of a Typical LMFBR Used in the Analysis.

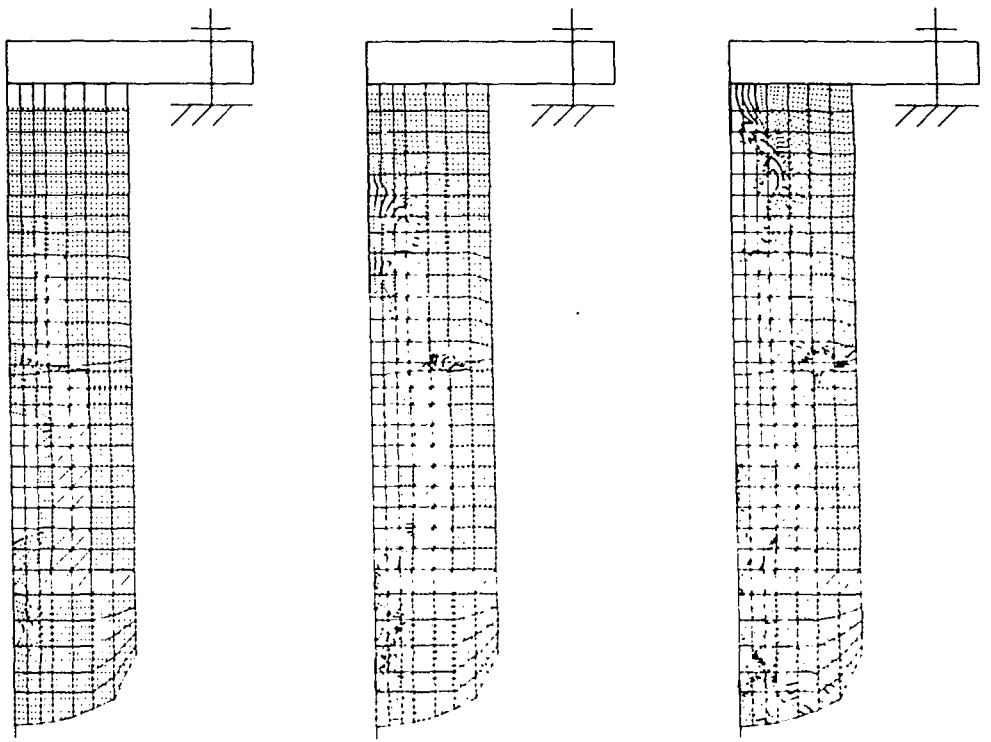

Fig. 11. Reactor Configurations at Three Different Times.

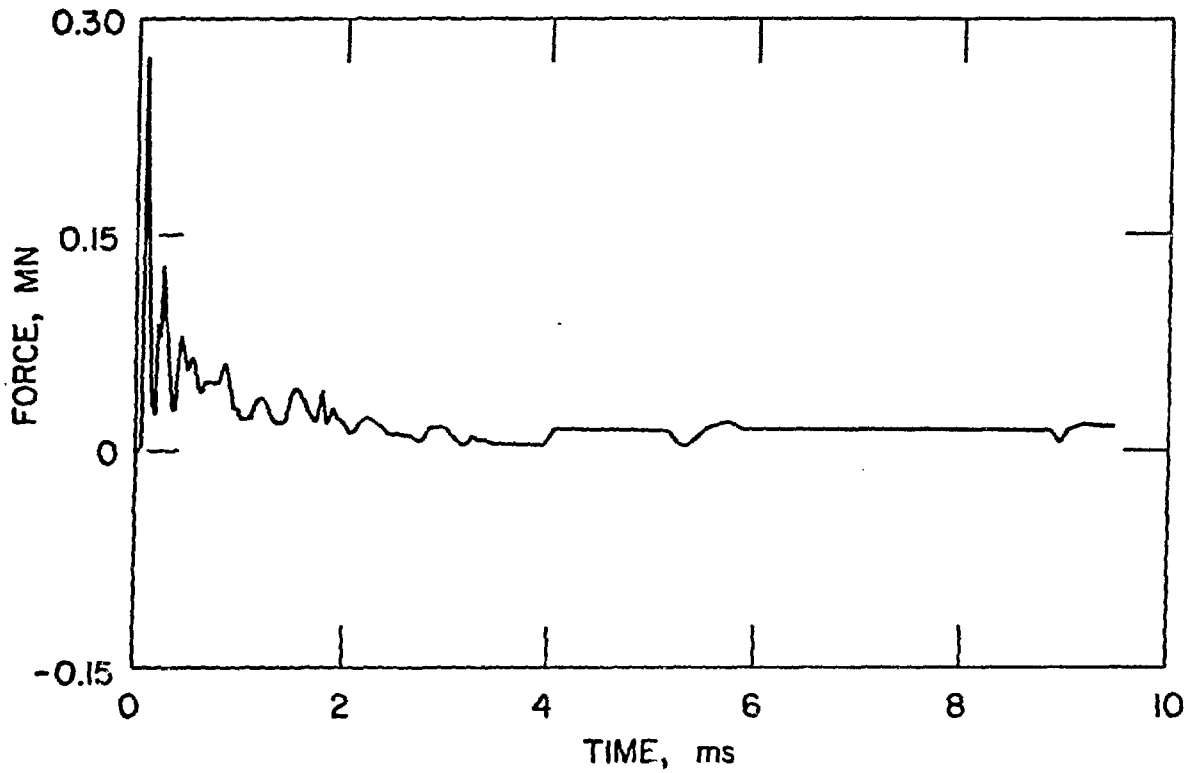

Fig. 12. Total Force on the UIS as a Function of Time.

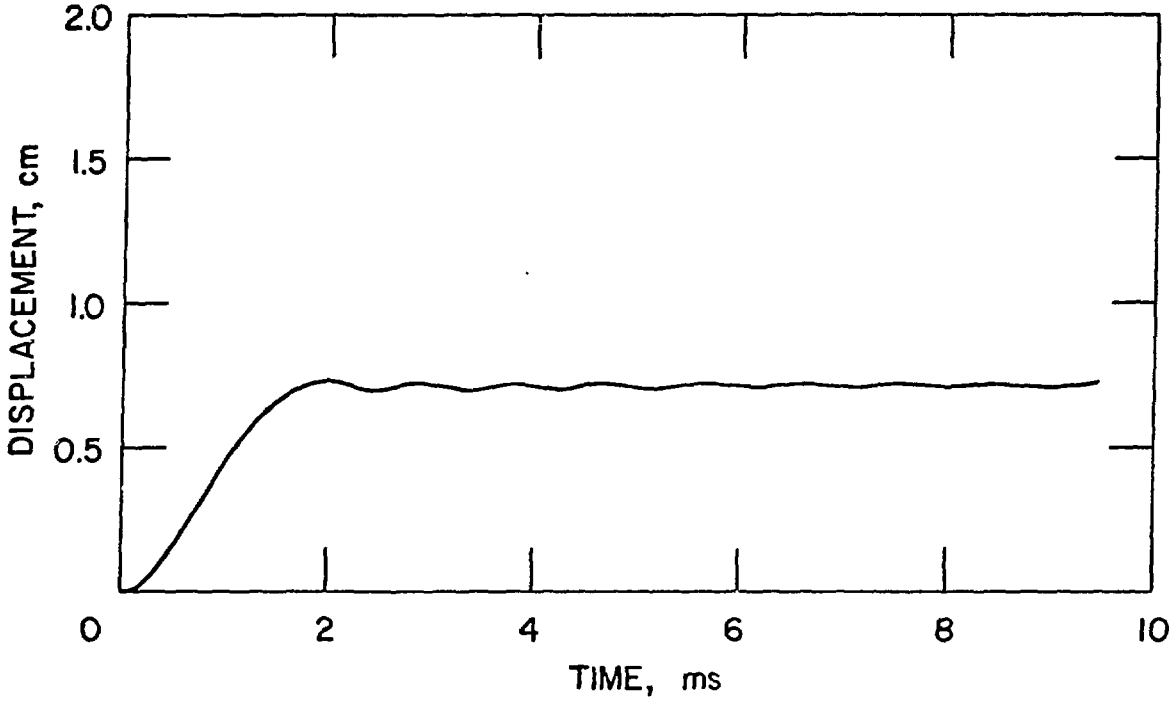

Fig. 13. UIS Displacement as a Function of Time.